Blood Flow in Channel Constrictions: A Lattice-Boltzmann Consistent Comparison between Newtonian and Non-Newtonian Models

G. A. Orozco[1†], C. T. Gonzalez-Hidalgo[2], A. D. Mackie[3], J. C. Diaz[4] and D. A. Roa Romero[1]

[1] *Faculty of Sciences, Physics Department, Universidad Antonio Nariño, Carrera 3 Este No 47 A–15, 110231 Bogotá, Colombia*
[2] *Industrial Engineering Department, Pontificia Universidad Javeriana, Carrera 7 No 40–62, 110231 Bogotá, Colombia*
[3] *Chemical Engineering Department, ETSEQ, Universitat Rovira i Virgili, Av. dels Països Catalans 26, 43007 Tarragona, Spain*
[4] *GTM, Department of Planning, Carrera 46 No 91-71. 110211 Bogotá, Colombia*

†Corresponding Author Email: gustavo.orozco@uan.edu.co

ABSTRACT

Lattice Boltzmann simulations have been carried out in order to study the flow of blood in normal and constricted blood channels using Newtonian and non-Newtonian rheological models. Instead of using parameters from previous works as is usually done, we propose a new optimization methodology that provides in a consistent manner the complete set of parameters for the studied models, namely Newtonian, Carreau-Yassuda and Kuang-Luo. The optimization was performed simultaneously using experimental data from several sources. Physical observables such as velocity profiles, shear rate profiles and pressure fields were evaluated. For the normal channel case, it was found that the Newtonian model predicts both the highest velocity and shear rates profiles followed by the Carreau-Yassuda and the Kuang-Luo models. For a constricted channel, important differences were found in the velocity profiles among the studied models. First, the Newtonian model was observed to predict the velocity profile maximum at different channel width positions compared to the non-Newtonian ones. Second, the obtained recirculation region was found to be longer for the Newtonian models. Finally, concerning the constriction shape, the global velocity was found to be lower for a rectangular geometry than for a semi-circular one.

NOMENCLATURE

c	speed of sound	$\dot{\gamma}$	shear rate
$\mathbf{e}$	lattice-boltzmann (LB) canonical velocity vector		
f	LB distribution function	ε	Knudsen number
f^{eq}	LB equilibrium distribution function	μ_∞	viscosity at infinite shear rate
p	pressure	ν	kinematic viscosity
Re	Reynolds number	σ_y	yield stress
$\mathbf{u}$	fluid velocity	ρ	density
w	LB weighting factor	τ	LB relaxation time

1. INTRODUCTION

Blood plays several fundamental roles in human and animal organisms. For instance, it transports oxygen and nutrients to the tissues, carries the metabolism products, protects the body from infections, participates actively in the hemostatic process, among many others. From a physical point of view

blood can be characterized through certain hemodynamic variables such as apparent viscosity, shear stress, shear rate as well as its fluid behavior through arteries, veins or vessels. Indeed, changes in these variables can produce alterations of the flow pattern, the way the blood components are delivered to an injured site and the flow conditions near the vessel wall. (Hathcock, 2006) Additionally, if the shear forces are not strong enough, blood viscosity can be increased due to the aggregation of erythrocytes and platelets. (Baskurt and Meisleman, 2003) All these phenomena might be associated with certain types of vascular diseases.

The flow behavior of blood has been studied both experimentally and computationally. For the first case, some works have reported experimental velocity profiles of blood flowing in a live vessel by way of techniques based on fluorescent markers or fluid nanoparticles. Such markers are inserted into the veins of live specimens such as rats or rabbits. The velocity distribution of blood can be obtained by recording several images and then by reconstructing the marker time trajectories.(Tangelder, Slaaf, Muijtjens, Arts, and Reneman, 1986; Ha, 2012) Another approach consists in studying the blood flow using computational algorithms through the Navier-Stokes equations (NSE) and assuming a rheological model. There are several different available methodologies that allow to numerically study the NSE. One of them, based on the transport Boltzmann equation, is the Lattice-Boltzmann (LB) method. (Succi, 2001) LB is an explicit method in which the dynamics of a fluid is modeled using a set of interacting particles located in a discretized space and with a set of associated probability distribution functions that allows us to recover the macroscopic variables such as density, momentum and energy. Besides the LB method, other blood flow studies have been performed using more classical approaches such as finite elements, (Weller, 2008; Weller, 2010) finite volumes (Sorensen, Burgreen, Wagner, and Antaki, 1999a; Sorensen, Burgreen, Wagner, and Antaki, 1999b) and finite differences. (Fogelson and Guy, 2004; Anand, Rajagopal and Rajagopal, 2005; Lobanov and Staroszhilova, 2005) Some attempts towards including explicitly the red blood cells have also been proposed using, for instance, smoothed particle dynamics, (Wootton, Popel, and Alevriadou, 2002) multiscale simulations, (Xu, Chen, M., Rosen, and Alber, 2008) mean field theory (Pivkin and Karniadakis, 2008) and the cellular automata approach. (Ouared and Chopard, 2005)

From a rheological point of view, blood viscosity presents interesting features such as shear thinning where viscosity can drastically change from an almost constant value at high shear rates to a significantly higher value at low ones. During a cardiac cycle the shear rate can change from 0 to 1000 s^{-1}, (Cho and Kensey, 1991) and so viscosity variations should be accounted for by using a constitutive equation. Different works have focused on studying the flow of blood using different models. For instance, Ashrafizaadeh and Bakhshaei (2009) studied the flow of blood using two dimensional LB

simulations and three non-Newtonian rheological models obtaining velocity profiles deviations between the Newtonian and non-Newtonian models. Boyd *et al.* (2007). studied the flow of blood in steady and oscillatory flows using two different non-Newtonian models. (Boyd, Buick, and Green, 2007) They found that the largest deviation from a Newtonian behavior is given by the Casson model. Bodnár *et al.* performed numerical simulations to compare the shear-thinning and the viscoelastic behavior of blood as a function of the flow rate, using the Carreau-Yasuda and Oldroyd-B models. They found that the shear-thinning effects are more pronounced than the viscoelastic ones. (Bodnár, Sequeira, and Prosi, 2011) Sorensen *et al.* (1999a) considered platelet deposition and thrombus formation over a collagen surface assuming a Newtonian fluid and neglecting the effect of an obstacle on the flow field. (Sorensen, Burgreen, Wagner, and Antaki, 1999a) Other studies have found relationships between the blood cell concentration (hematocrit), the wall shear rate, and the wall shear stress. (Box, van der Geest, Rutten, and Reiber, 2005)

Despite the fact that the Casson model has been widely studied, there is no agreement with respect to its range of validity. While some studies (Milnor, 1982) state that it is only valid at shear rates $\leq 10\mathrm{s}^{-1}$ other studies (Bate, 1977) have reported ranges between 15 to 6400 s^{-1} or hematocrit concentrations $\leq 40\%$. (Wang, 2011) Indeed, as will be shown in section 3.2, the Casson model does not provide a satisfactory fit of the experimental data when the whole range of shear rates is considered.

As mentioned above, previous works have studied the flow behavior of blood using different rheological models. For instance, Ashrafizaadeh *et al.* compared the C-Y, K-L and Casson models using experimental measurements of a thiocyanate solution (blood-mimicking fluid) for the C-Y model (Gijsen, van de Vosse, and Jansenn, 1999; Gijsen, Allanic, van de Vosse, and Jansenn, 1999) and human blood for the K-L and Casson models (Luo and Kuang, 1992) This comparison is in principle not consistent because of the different nature of the data. On the other hand, Boyd *et al.* (2007) made comparisons between the Casson and the C-Y models performing independent fits on the same sample. Nevertheless, we consider this procedure to be also flawed, since the viscosity at infinite shear rate is a parameter that couples all model equations. Such a coupling is clearly unaccounted for when fits are performed independently. Consequently, these procedures might not provide reliable conclusions and thus, for the sake of a consistent comparison, we propose to determine the parameters for all models using a simultaneous fit given a unique set of experimental data. To our knowledge, this issue has not yet been considered and therefore deserves a detailed study.

In this work several features will be addressed, namely: i) a new set of parameters are needed for the Carreau-Yassuda (C-Y) and the Kuang-Luo (K-L) models. To do so, a simultaneous fit for the two models is performed using the same set of

Table 1 Rheological models equations and numerical values of the parameters

Model	Equation	Parameters					Reference
		a	n	μ_0 (Pa s)	μ_∞ (Pa s)	λ (s)	
C-Y	$\dfrac{\mu - \mu_\infty}{\mu_o - \mu_\infty} = (1 + (\lambda\dot\gamma)^a)^{\frac{(n-1)}{a}}$	0.644	0.392	22.00×10^{-3}	2.20×10^{-3}	0.11	(Ashrafizaadeh and Bakhshaei 2009)
		0.640	1.790	160.0×10^{-3}	3.60×10^{-3}	8.20	(Bodnár, Sequeira, and Prosi 2011)
		1.250	0.220	56.00×10^{-3}	3.45×10^{-3}	1.90	(Cho and Kensey 1991)
		0.640	1.790	160.0×10^{-3}	3.50×10^{-3}	8.20	(Leuprecht and Perktold 2001)
		1.700	1.510	13.15×10^{-3}	3.00×10^{-3}	0.50	(Perktold, Peter, and Resch 1995)
		5.510	0.450	64.01×10^{-3}	2.66×10^{-3}	8.50	This work
K-L	$\mu = \mu_\infty + \dfrac{\eta}{\sqrt{\dot\gamma}} + \dfrac{\sigma_y}{\dot\gamma}$	μ_∞(Pa s)		σ_y (Pa)		η(Pa s$^{1/2}$)	
		4.076×10^{-3}		4.968×10^{-3}		16.07×10^{-3}	(Luo and Kuang 1992)
		2.66×10^{-3}		0.170×10^{-3}		18.70×10^{-3}	This work

experimental samples, ii) a comparison between the rheological models is established using this new set of parameters, iii) a physical obstacle is placed on the vessel wall in order to find out its effect on the velocity and shear rate profiles for each rheological model, and finally iv) the length of the re-circulation region is studied as a function of the obstacle size.

This paper has been divided as follows. In the second section, the computational details of the simulations are given. In the third section, the results are discussed beginning with the parameters obtained after our fitting procedure. Afterwards, a comparison of the rheological models in a vessel with and without a semi-circular obstacle is given. Then, the effect of the semi-circular obstacle for different sizes on the velocity profiles, shear rates and the length of the re-circulation region, is studied. Finally, for the Newtonian case, a comparison between two different obstacle geometries is also established.

2. COMPUTATIONAL FEATURES AND NUMERICAL PARAMETERS

Figure 1 shows an schematic representation on the studied geometry. The flow of blood was computationally studied by simulating a channel section of width 4 mm and 60 mm length, (Glaser, 2012) using two dimensional LB simulations. Specifically, velocity profiles, shear rates, shear stresses and pressure fields were determined along the section. The non-Newtonian behavior of blood was accounted for by using two non-rheological models which will be described in the next section and whose constitutive equations can be found in Table 1. LB is an explicit method in which the dynamics of a given fluid is obtained from a set of particles located in cells defining a lattice geometry. Particles can either remain in a given cell or migrate to neighbor lattice sites following Q possible directions, according to a probability function. For the present study, the D2Q9 model was used, where Q indicates the nine possible spatial directions and D the number of spatial dimensions, which for our case is two.

It is then possible to define f_i as the streaming probability distribution in the *i-th* direction. f_i evolves through time for every cell in the lattice according to Eq. (1):

$$f_i(x + e_i\Delta t, t + \Delta t) - f_i(X,t) = -\frac{1}{\tau}(f_i(X,t) - f_i^{eq}(X,t)) \qquad (1)$$
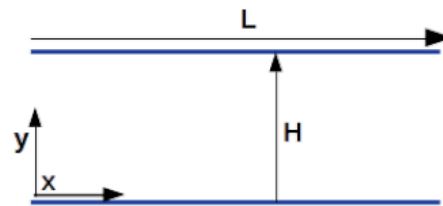

Fig. 1. Sketch of the channel geometry and coordinates system.

where τ represents a relaxation parameter usually considered to be in the range $1/2 < \tau \le 1$, $\mathbf{e}_i$ is a velocity vector pointing to the i − th direction and f^{eq} is the equilibrium probability distribution. Eq. (1) represents two processes: collision and streaming. The r.h.s represents the collision operator that considers the difference between the current distribution and the equilibrium one in a time interval τ. The l.h.s represents the streaming of the particles to the neighbor cells. The equilibrium distribution function f^{eq} is defined by Eq. (2)

$$f_i^{eq} = w_i\rho\left(1 + 3\frac{e_i\mathbf{u}}{c^2} + \frac{9}{2}\frac{(e_i.\mathbf{u})^2}{c^4} - \frac{3}{2}\frac{u^2}{c^2}\right) \qquad (2)$$

where c corresponds to the speed of sound, w_i is a weighting factor, ρ the fluid density and $\mathbf{u}$ the average particle velocity in each cell. Eq. (1) involves an iterative process where the distribution function is updated every time step until the equilibrium is satisfied, i.e., the l.h.s of Eq. (1) is equated to zero. Due to the fact that zero cannot be numerically reached, in this study simulations are considered finished as long as the criterion given by Eq. (3) is satisfied,

$$\sum_k \frac{\|u_k(t + \Delta t) - u_k(t)\|}{u_k(t + \Delta t)} \le 10^{-9} \qquad (3)$$

where $\mathbf{u}_k$ corresponds to the velocity in the lattice site k and the summation is performed over the whole lattice. Lattice size effects were checked with bigger lattices obtaining similar results within the statistical uncertainties. Longer simulations were also performed to obtain 10^-10 in the criterion value, and

similar results were obtained.

Bounce back boundary conditions were used to reproduce the channel walls that were considered to be rigid regardless of the blood pressure. For these conditions, the components of the incoming velocity on the wall are propagated in the opposite direction defining a non-slip condition. At the inlet-outlet of the channel, pressure boundary conditions were used as proposed by Zou and He (1997) Density and pressure are related through $p = \rho \dfrac{c^2}{3}$ and the Reynolds number is defined by eq-4

$$Re = \frac{c^2}{36v^2} \frac{\Delta\rho}{\rho} \frac{H^3}{L} \qquad (4)$$

where H and L are the channel width and length and $v = \mu_\infty/\rho$ is the kinematic viscosity. Eq. (4) allows a pressure gradient to be imposed once the Reynolds number is fixed. For non-Newtonian models, viscosity is not a constant value and so in order to determine Re the v value is considered as the limiting viscosity at infinite shear rate, μ_∞, which is the coupling parameter for all the constitutive equations and can be obtained from a simultaneous fit of the experimental data. Based on reported values for channels of 4 mm, (Glaser, 2012) for all simulations a Reynolds number of 500 was chosen. According to Eq. (4) this Reynolds number defines a pressure difference of 1.19×10^{-3} in LB units. The relaxation parameter τ is a function of the kinematic viscosity v defined by Eq. (5):

$$\tau = 3v + \frac{1}{2} \qquad (5)$$

As already known, when considering a non-Newtonian behavior, v and τ become a function of the shear rate $\dot\gamma$. Therefore, new constitutive models that relate them must be used. Following Krüger *et al.* $\dot\gamma$ is calculated through Eq. (6) . (Krüger, Varnik, and Raabe, 2009)

$$\dot\gamma = -\frac{3\Pi^{(1)}}{\tau\rho} \qquad (6)$$

where $\Pi^{(1)}$ is defined as $\sqrt{\Pi_{\alpha\beta}^{(1)} \Pi_{\alpha\beta}^{(1)}}$ and $\Pi_{\alpha\beta}^{(1)}$ is a second rank tensor related to the momentum flux at the macroscopic level defined by Eq. (7)

$$\Pi_{\alpha\beta}^{(1)} = \sum_i c_{i\alpha} c_{i\beta} f_i^{(1)} \qquad (7)$$

where $f_i^{(1)}$ refers to the second term in the expansion of the distribution function around the equilibrium, defined in Eq. (8) :

$$f_i = f_i^{(0)} + \varepsilon f_i^{(1)} + \varepsilon^2 f_i^{(2)} + O(\varepsilon^2) \qquad (8)$$

From this expression, $f_i^{(0)} = f_i^{eq}$ and the distribution function out of equilibrium is $f_i^{neq} \approx f_i^{(1)} \approx f_i - f_i^{eq}$ being ε the Knudsen number. Eq. (6), along with the constitutive equations, are needed to obtain $\dot\gamma$ and to calculate v

and τ. The obtained system of equations given by $\dot\gamma$ and v can be solved either analytically or numerically depending on the rheological model that for this work corresponds to the C-Y (Robertson, Sequeira, and Owens, 2009) and the K-L (Luo and Kuang, 1992) models. In particular, the K-L model allows an analytical solution to be found while the C-Y model requires the solution of a non-linear system of equations that was solved using the Newton-Raphson method.

The momentum flux tensor $\Pi_{\alpha\beta}^{(1)}$ was used to obtain the physical quantities for every lattice cell such as the strain and shear rate magnitudes. Alternatively, shear rates were also calculated through a second order finite difference scheme over the velocity profiles. Although locality is lost using this methodology, comparable results can be also obtained. However, the lattice resolution should be modified for the majority of cases through the parameters Δx and Δt.

The pressure field along the studied channel was calculated using the LB distribution given by Eq. (9) (Kürger, Varnik, and Raabe 2009)

$$p = -\rho u^2 + \Pi^{(0)} \qquad (9)$$

with $\Pi^{(0)}$ defined similarly as $\Pi^{(1)}$ in Eq. (7) .

A lattice of 200×3000 square cells was used for all simulations, with $\Delta x = 2 \times 10^{-5}$ m and $\Delta t = 2 \times 10^{-6}$ s. This has been tuned by comparing the theoretical velocity profiles for non-obstacle cases with those obtained by simulation, except for the case of the C-Y model where there is no analytical solution.

In order to study the behavior of the blood flow around a blood clot, an obstacle was introduced at the bottom wall of the channel centered at $\sim$ 27% the channel length (16mm). Subsequently, the obstacle size was changed in order to establish its effect over the different profiles. The obstacle geometry was also considered including both semi-circular and rectangular geometries. The obstacle cells do not perform neither collision nor streaming steps and bounce back boundary conditions were assumed. Four different semicircular sizes of radius 40, 80, 120 and 160 Δx were studied, which corresponds to 20, 40, 60 and 80% of the channel width. A rectangular obstacle of 80 Δx length was also considered in order to establish possible differences between the geometries.

Numerical simulations were performed using our in-house code developed from scratch in the C++ language and parallelized using the OpenMP libraries. Computing time can be significantly affected depending on the lattice size and the rheological model. For instance, a simulation in a lattice of 200 × 3000 using a Newtonian model without an obstacle takes around 60 hours using 4 intel Xeon processors at 2.5 *GHz*, while for a non-Newtonian model simulations require about 20% more time. The computing time was found to increase by approximately three when introducing a semi-circular obstacle of 80% the channel width.

3. RESULTS

3.1 Simultaneous Optimization of the Rheological Parameters

The use of different parameters sets can cause a bias in the analysis when comparing more than one rheological model. This inconsistency makes it difficult to conclude that any difference found between the models is due to the blood behavior. Thus, as mentioned in the Introduction, in this work all the parameters were fitted using the same experimental samples. The only requirement to do so is to include a coupled parameter between the models which, as can be seen in Table 1, corresponds here to the viscosity at infinite shear rate (μ_∞). Note that both the K-L and the C-Y models reproduce this value in the high shear rate limit. To the best of our knowledge no previous works have considered this issue.

The optimization procedure we propose requires the minimization of an objective function defined by Eq. (10):

$$F = \frac{1}{n} \sum_{i=1}^{n} \left[\frac{(\mu_i^{est-KL} - \mu_i^{exp})^2}{s_i^2} + \frac{(\mu_i^{est-CY} - \mu_i^{exp})^2}{s_i^2} \right] \tag{10}$$

where *n* is the total number of experimental data used for the fitting procedure (a total of 33 data were used (Brooks, Goodwin, and Seaman 1970; Chien, Usami, M., L., and Gregersen, 1966; Chien, 1970; Skalak, Keller, and Secomb 1981)), μ_i^{est} corresponds to the estimation of viscosity obtained using the rheological models, mu_i^{exp} represents the experimental viscosity and s_i^2 is the associated uncertainty of the experimental data. *F* is an implicit function of $\{y_j\}$ that represents the set of rheological parameters to be fitted which corresponds to the C-Y and K-L models given by $\left\{y_j^{C-Y}\right\} = \left\{\mu_\infty, \mu_0, \lambda, n, a\right\}$ and $\left\{y_j^{K-L}\right\} = \left\{\mu_\infty, \eta, \sigma_y\right\}$ respectively.

The idea is to minimize *F* with respect to every parameter $\{y_j\}$. Thus, from the differentiation of eq-10, it is possible to find Eq. (11):

$$\frac{\partial F}{\partial y_j} =$$

$$\frac{1}{n} \sum_{i=1}^{n} \frac{2(\mu_i^{est-KL} - \mu_i^{exp})}{s_i^2} \frac{\partial \mu_i^{est-KL}}{\partial y_j} + \tag{11}$$

$$\frac{2(\mu_i^{est-CY} - \mu_i^{exp})}{s_i^2} \frac{\partial \mu_i^{est-CY}}{\partial y_j}$$

Since the initial values are unknown for both models, it is necessary to make a first order Taylor expansion of μ_i^{est} around the initial guess $\left\{y_j^0\right\}$ obtaining Eq. (12)

$$\mu_i^{est}(y_j^0 + \Delta y_j) \approx \mu_i^{est}(y_j^0) + \sum_{j=1}^{p} \frac{\partial \mu_i^{est}}{\partial y_j} \Delta y_j$$

$$i = 1,...,n \tag{12}$$

where $\Delta y_j = y_j - y_j^0$ and *p* is the number of parameters to be fitted that depends on the rheological model to be used. For instance, in the C-Y model, four parameters need to be considered, namely $\lambda, n, a, \mu_\infty$. Derivatives $\frac{\partial F}{\partial y_k}$ can be explicitly calculated from the rheological equations given in Table 1.

Replacing Eq. (12) into Eq. (11) it is finally obtained that

$$0 = \sum_{i=1}^{n} \left[\frac{\left(\mu_i^{est-KL}(y_j^0) - \mu_i^{exp}\right) + \sum_j \frac{\partial \mu_i^{est-KL}}{\partial y_j}(\Delta y_j)}{s_i^2} \frac{\partial \mu_i^{est-KL}}{\partial y_j} + \frac{\left(\mu_i^{est-CY}(y_j^0) - \mu_i^{exp}\right) + \sum_j \frac{\partial \mu_i^{est-CY}}{\partial y_j}(\Delta y_j)}{s_i^2} \frac{\partial \mu_i^{est-CY}}{\partial y_j} \right] \tag{13}$$

Eq. (13) represents a square linear system of the form $\mathbf{A}\Delta\mathbf{y_j} = \mathbf{B}$ with 7 unknowns that represent the parameters to be simultaneously estimated ($y_1, y_2, ... y_7$). Since the minimization requires several trials, the matrix construction and solution were implemented in our in-house code using the lower-upper (LU) decomposition method. The optimized parameters obtained after an iterative procedure are presented in Table 1.

As a first approach, independent fits of every model can be performed keeping the coupling parameter µ∞ as a fixed value. Nonetheless, when following this procedure the obtained parameters are different from the simultaneous fit. Moreover, the value of the objective function for the total set of data is also greater indicating that this procedure does not give the optimal solution. The reason for these different results is related to the fact that using such an approach, the system degrees of freedom are reduced. However, the parameters obtained from the independent fits can be used as initial guesses for the simultaneous fit.

3.2 Rheological Model Parameters

As mentioned before, we considered several rheological models, namely, Newtonian, C-Y and K-L. Parameters of every model were simultaneously obtained from a fit of experimental viscosities reported from different works. Namely, Brooks *et al.* reported viscosity data using suspensions of erythrocytes (RBC) in saline and plasma. (Brooks, Goodwin, and Seaman 1970) Chien *et al.* (1966) reported measurements using blood and suspensions of RBC in plasma (Chien, Usami, and Gregersen, 1966) as well as in Ringer solutions with albumin at 45% of RBC concentration (Chien, 1970) and finally

the reported values by Skalak *et al.* (1981) which are also 45% of RBC concentration. There are more available experimental samples but the RBC concentration is out of the range of the above-mentioned studies, for instance Zydney, Oliver III, and Colton (1991) and Biro (1982) reported measurements using RBC concentrations of around 98% and 18-22% respectively.

Table 1 shows the constitutive equations corresponding to each rheological model, the parameters reported by previous computational studies as well as our proposed set of new parameters obtained from the simultaneous fit. The observed numerical differences between the parameters might be attributed to the use of different experimental samples, experimental set up or experimental conditions.
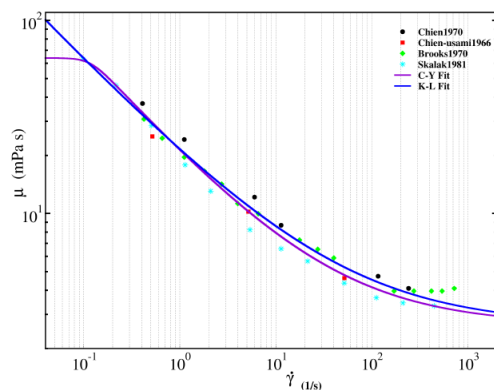

Fig. 2. Viscosity as a function of γ̇. Symbols represent experimental data, violet line the C-Y fit and continuous blue line the K-L fit.

Figure 2 shows the viscosity behavior as a function of the shear rate for each rheological model obtained after the fit. Experimental data are also shown and correspond to experimental samples.

It is important to mention that the Casson model was initially considered in this study. This model was originally developed for characterizing inks and is generally used to describe certain types of food. (Casson, 1959) Two parameters are involved: the limit viscosity at high shear rates μ_∞ and the shear yield σ_y. Although this model is able to fit the experimental data proposed by Biro, (1982) when more data samples are included (specially $\dot{\gamma} \leq 2s^{-1}$) it was not possible to obtain a reasonable adjustment for the whole $\dot{\gamma}$ range. A possible reason of the poor fit could be related to the fact that the Casson model only has two adjustable parameters which additionally are not independent.

Unlike the Casson model where a discontinuity exists at $\dot{\gamma} \to 0$, the C-Y model describes blood for the whole $\dot{\gamma}$ range. This model defines two limit viscosities at low and high $\dot{\gamma}$ which correspond to μ_0 and μ_∞ respectively. Figure 2 shows the viscosity behavior of blood as a function of $\dot{\gamma}$. The violet line corresponds to the C-Y model; as shown, this model presents both a plateau (low $\dot{\gamma}$) and an asymptotic behavior (high $\dot{\gamma}$). Besides the limit viscosities, three

additional parameters (λ, a, n) that govern the plot shape are required (see Table 1). λ can be associated with the relaxation time, i.e., the time needed for a set of red blood cells to form an aggregate or roleau. (Fedosov, Wenxiao, Caswell, Gompper, and Karnidiakis, 2011; Liu and Liu, 2006; Zhang and Neu, 2009) The greater the λ the lower the tendency to form a roleau. In terms of parameter sensitivity, an increase in λ implies a reduction in the plateau length indicating that it is more difficult to create a roleau and therefore the viscosity tends to be lower. With regards to a and n, they are able to change both the slope and the smoothness in the transition region defined between the low and the high viscosity limit values. The blue line corresponds to the K-L model which is a modification of the Casson equation. The K-L model introduces a new parameter η that helps to provide a better description of the shear thinning behavior at low $\dot{\gamma}$ values where, as mentioned before, the Casson model fails.

3.3 Comparison between the Rheological Models. Non-Obstacle case

Figures 3-a and 3-b show the velocity and shear rate profiles for every rheological model, both profiles are normalized with respect to the maximum velocity of the Newtonian model. Channel width is also shown in normalized units. Continuous black, red and blue lines correspond to the Newtonian, C-Y and K-L models respectively. As expected, for all velocity profiles maxima are located at the channel center. From highest to lowest, velocity predictions were given by the Newtonian, the C-Y and the K-L model respectively. Quantitatively, C-Y and K-L predict $\sim$ 30% and $\sim$ 37% lower values than the Newtonian model. Concerning the peak shapes, it is possible to observe that the non-Newtonian models present flatter profiles around the maximum being slightly more pronounced for the K-L model. This result is consistent with the shear rate profiles provided in Figure 3-b where non-Newtonian models have a concave-up and smoother behavior around the channel center, contrary to the Newtonian shear rate profile where a non-smooth curve can be identified.

The highest shear rates are located at the channel walls and, in terms of percentages, the C-Y and K-L models are respectively $\sim$ 20% and $\sim$ 35% lower than the Newtonian model. Note that, although the viscosity behavior as a function of $\dot{\gamma}$ (see Figure 2) is relatively close for both models, and the velocity profiles are also close to each other, the C-Y model predicts shear rates $\sim$ 20% higher than the K-L model. Considering the fact that all models have the same μ_∞ value, these results indicate that a Newtonian assumption might lead to overestimate these results. In fact, according to the experimental work carried out by Tangelder *et al.* (1986) a parabolic profile tends to overestimate the velocities at the center of the channel. (Tangelder, Slaaf, Muijtjens, Arts, and Reneman, 1986) Concerning the non-Newtonian models, the obtained results indicate that experimental data of viscosity are not enough to determine the model that best describes the flow of blood and therefore additional experimental measurements of other physical observables are needed.

Despite the fact our velocity profiles follow the same trend reported by Ashrafizaadeh *et al.,* in all cases our simulations predict numerically higher velocity values. Also, our obtained differences between the non-Newtonian models are far lower, especially for the K-L model where our region around the channel center is much less flat. This disagreement is related to the fact that in the work of Ashrafizaadeh *et al.*, the C-Y and K-L models have different μ_∞ values and therefore a direct comparison cannot be established since they correspond to two different blood samples.
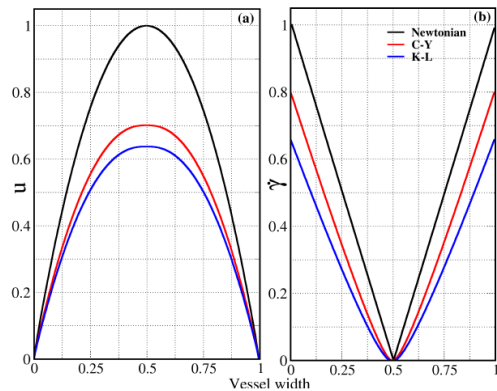
Fig. 3. Comparison of velocity and shear rate profiles for the different rheological models. Channel width is shown in normalized units (a) normalized velocity profiles (b) normalized shear rate profiles. Normalization is based on the Newtonian values.

3.4 Comparison between the Rheological Models. Obstacle Case

For the majority of arteries, if there are no obstructions or abrupt walls and the shear rate is high enough, blood can behave as a Newtonian fluid. However, around stents and thrombi in the channel non-Newtonian behavior of blood can be found.

Some authors have studied the flow of blood considering the thrombus formation through a complex set of chemical reactions. For instance, Sorensen *et al*. (Sorensen, Burgreen, Wagner, and Antaki 1999a) assumed a Newtonian behavior neglecting the thrombus effect on the flow. Our interest is precisely to quantify the obstacle effect on the velocity profiles and the re-circulation region. Chemical reactions will not be accounted for, and hence the obstacle effect will be only treated from a physical point of view. To do so, a semi-circular obstacle will be placed on the bottom wall of the channel and its size will be subsequently increased in order to create a dynamical channel constriction.

Figure 4 shows the obstacle effect on different variables using a Newtonian model. Namely, the velocity profiles Fig.4-(a), the shear rates profiles Fig. 4-(b) and the pressure field Fig. 4-(c) are presented. For this particular Figure, the obstacle radius corresponds to 40% of the channel width. For visualization purposes only part the normalized channel length is shown. From Fig. 4-(a) it is

possible to see a vertical displacement of the maximum velocity region (red color) as well as a recirculation region just after the obstacle (dark blue color). As shown in Fig. 4-(b) most parts of the channel are governed by low shear rate regions. However, high shear rate regions can be identified over the obstacle as well as at the top wall of the channel, being higher above the obstacle. Fig. 4-(c) shows the pressure field inside the channel. As can be appreciated, there is a minimum of pressure just above the obstacle whose magnitude is even lower than the one obtained at the channel outlet. This global minimum is defined by two pressure gradients, one of them located in the region before the obstacle and related to the channel constriction that makes the fluid speed up, and another one in the region after it and related to the velocity reduction.

The effect of the rheological model was also studied, however differences are difficult to establish from a color map and therefore profiles as a function of the channel width were considered. Fig. 5-a, Fig. 5-b and Fig. 5-c show the normalized velocity profiles for all rheological models using an obstacle of radius 40% of the channel width. Velocity profiles were evaluated for different channel lengths in normalized units, namely, 0.2, 0.3, 0.5 and 1.0. Compared to the non-obstacle case, the velocity profiles have a similar trend, i.e., the Newtonian model predicts the highest velocity values followed by the C-Y and the K-L models. Nevertheless, velocity magnitudes are $\sim$ 12% lower compared to the non-obstacle case. Negative velocities as well as a displacement of the velocity profiles maxima can also be observed for all models at a length of 0.3 represented by the red lines. On the contrary, profiles after the obstacle (green and black lines) show the maximum velocity located at the center of the channel width. At lengths of 0.2 and 1.0 (blue and black lines) profiles are qualitatively similar but they are shifted slightly. Although a shift is expected, since the constriction reduces the cross-sectional area of flow, it is interesting to note that for the case without obstacle maxima are located at the same position independently of the rheological model. However, when an obstacle is considered, the Newtonian model predicts the maxima at different channel width positions than the non-Newtonian ones. This particular issue will be discussed later.

Figure 6 shows the effect of the obstacle size on the velocity profiles. Four different obstacle sizes were studied and correspond to radii of 20%, 40%, 60% and 80% the channel width. As previously done, the velocity values were normalized with respect to the maximum Newtonian velocity. For this particular case, simulations were required to satisfy the stricter condition of 10^{-10} in the equilibrium criterion given by Eq. (3) . The profiles shown are evaluated at 0.3 of the channel length. Although numerical differences were observed evaluating the profile at different lengths, a similar qualitative trend was found (not shown).

As the size increases, it is possible to see a reduction of the velocity that is more pronounced for the Newtonian model followed by the C-Y and the K-L models. Also, for all models, maxima are displaced as a function of the obstacle size, and negative
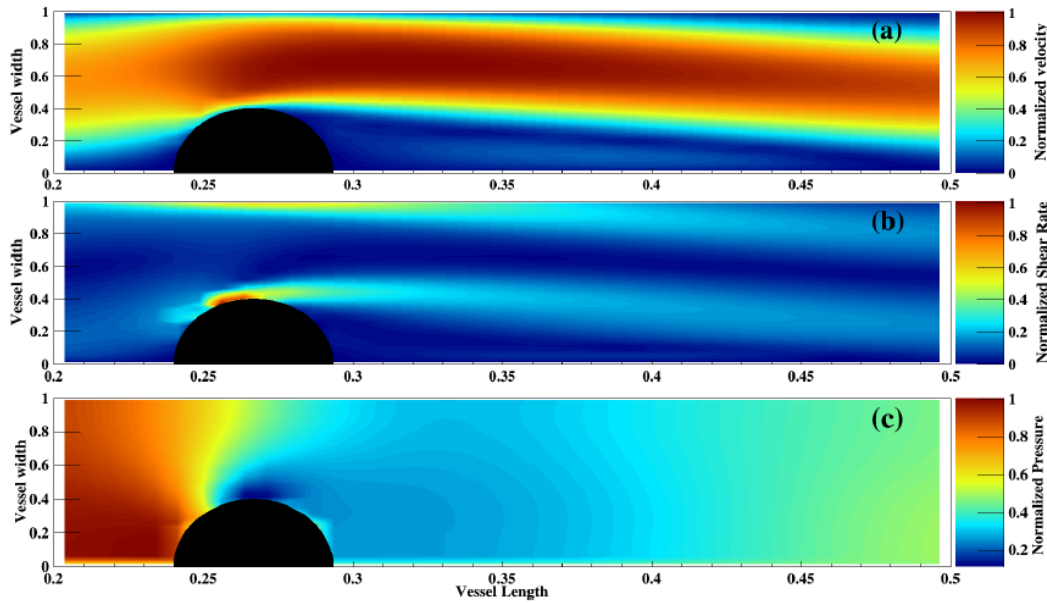
Fig. 4. Velocity, shear rates and pressure behavior for the Newtonian model in the presence of a semi-circular obstacle. Plots were coded in the ROOT data analysis framework. All values are shown in normalized units.
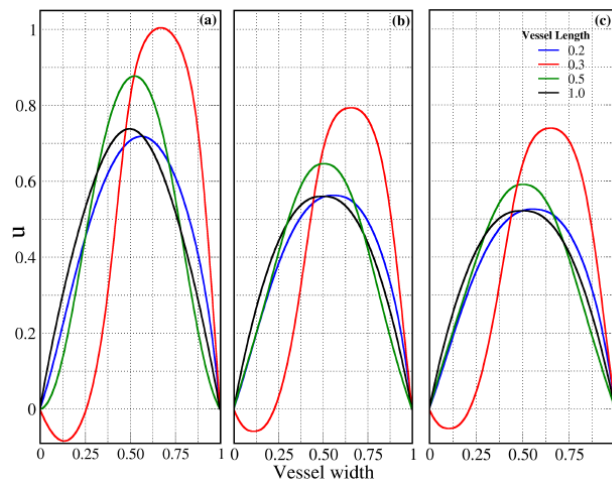

Fig. 5. Velocity profiles for the different rheological models using an obstacle of radius 40% of the channel width. (a) Newtonian model (b) C-Y model (c) K-L model. The profiles were taken at different normalized channel lengths before and after the obstacle.

velocities can be observed to be higher in magnitude for the Newtonian model. The origin of negative velocities is related to the existence of a recirculation region, which is produced by the contact between the fluid and the obstacle surface. This interaction reduces the fluid kinetic energy and avoids part of it to overcome the adverse pressure gradient.

Figure 7 quantifies some of the above-mentioned effects. Figure 7-a shows how the velocity maximum is reduced as a function of the obstacle size. All rheological models exhibit a similar trend with different slopes. All curves are bounded between two limits, namely, the upper limit for a system without an obstacle and the lower one for a complete obstruction. As can be observed, the Newtonian model has the steepest slopes for nearly all obstacles

sizes. This result can be explained due to the fact that the highest velocity values are predicted by the Newtonian model and for a complete constriction all models should converge to zero. Non-Newtonian models show a much less pronounced effect for the first two sizes. However, as the obstacle size increases, slopes start to be numerically closer. Differences between Newtonian and C-Y models are on average ∼ 25% while for K-L and the Newtonian model difference are on average ∼ 32%.

Figure 7-b, shows the position dependence of the velocity profiles maxima relative to the obstacle size at 0.3 of the channel length. The first point refers to the non-obstacle case where all maxima are located at the channel center. Contrary to Fig. 7-a, differences among the Newtonian and non-
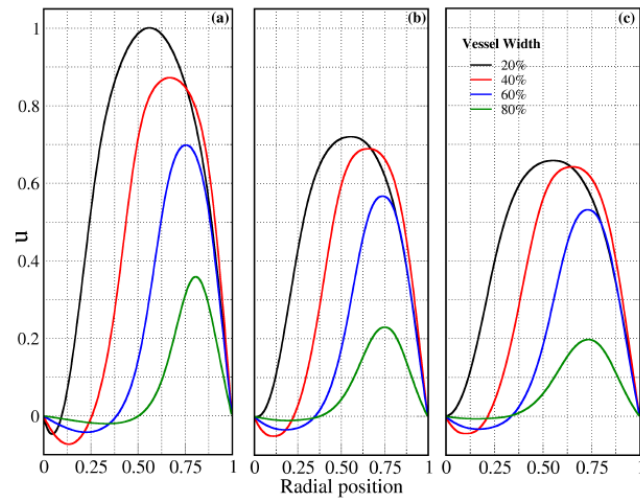
Fig. 6. Normalized velocity profiles as a function of the obstacle size, profiles were obtained at 0.3 the channel length.(a) Newtonian (b) C-Y (c) K-L.
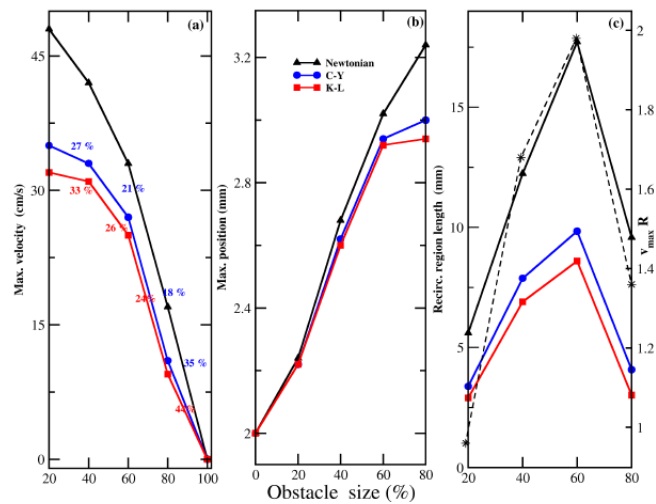

Fig. 7. Obstacle size effects at 0.3 the normalized channel length (a) Maximum velocity. The velocity reduction percentages are relative to the Newtonian model (b) Position of the maximum velocity (c) Size of the recirculation region (right scale) and vmaxR (left scale).

Newtonian models begin to be more noticeable for the second obstacle size and are slightly higher after this point. Note that differences between the C-Y and the K-L models are not significant. Figure 7-c shows a plot of the obstacle size and the length of the recirculation region. The recirculation region length is quantified by looking for the most distant cell from the right hand side of the obstacle having a negative horizontal component of the velocity. Results indicate that the Newtonian model predicts a region length ∼ 30 % longer compared with the non-Newtonian models. Additionally, a non-monotonic behavior defining a maximum between the 60% and 80% obstacle sizes can be also identified. In order to understand this behavior, Fig. 7-a can be considered again. Despite the fact that the bigger the obstacle the larger the velocity reduction (between two consecutive obstacles), there is no linear relation between them. Therefore, the product between vmax and R which is actually proportional to the Reynolds number is not a constant and follows the non-

monotonic behavior shown by the dashed black line in Fig. 7-c. Note that R corresponds to the semi-circular obstacle size and v_{max} to the maximum of the velocity profile. The fact that the trend of the other curves in Fig. 7-c is similar to the $v_{max} \times R$ trend is totally consistent since the recirculation length is intimately related to the Reynolds number.

Another studied effect corresponds to the shear rate. As is already known, the largest shear rates are expected to be at the wall channels as well as around the obstacle. Figure 8 shows the average shear rates values as a function of the obstacle size evaluated at four different lengths, namely: i) just before the obstacle (8-a) ii) over the center of the obstacle (8-b) and iii) just after the obstacle (8-c). Averages were obtained by taking into account the shear rate values across the channel width.

As the obstacle size increases, the average fluid velocity decreases in the whole channel which also implies a reduction in the fluid velocity maxima.
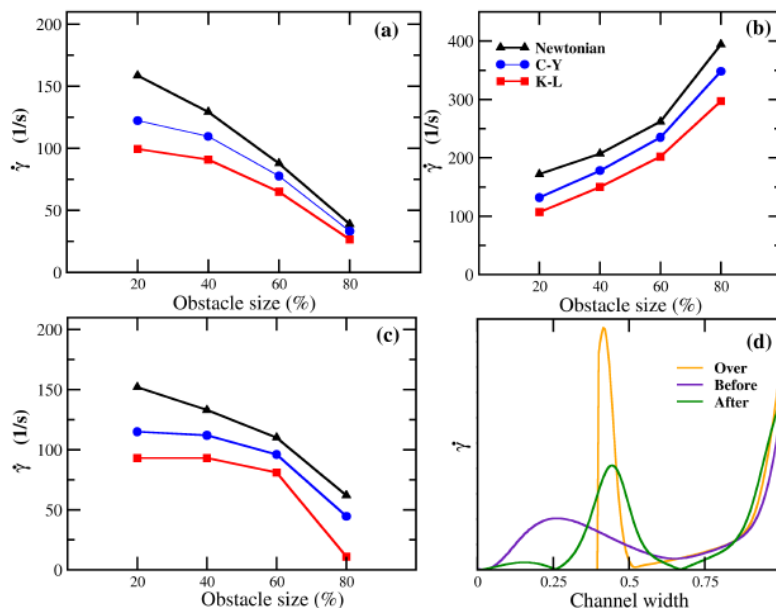
Fig. 8. Average shear rates around the obstacle region. (a) just before the obstacle (b) over the obstacle (c) just after the obstacle (d) qualitative shear rate profiles across the channel width.

Since the velocity remains zero at the channel walls and over the obstacle, both velocity changes and shear rates are lower as well. Fig. 8-a and Fig. 8-c show how the average shear rates decrease as a function of the obstacle size for regions away from the constriction. On the other hand, the largest velocities are located over the obstacle and define a velocity profile which drastically changes from the obstacle wall to the constriction center. As a consequence, the average shear rate is larger around the obstacle region and increases as a function of the obstacle size as shown in Fig. 8-b.

No major differences can be appreciated between the average shear rate inside and outside the constriction region for the smallest obstacle. Numerical values range between 100-180 s^{-1}. However, for the largest obstacle, at the constriction the average shear rates increase up to ~ 400 s^{-1} while away from it they are always lower than 80 s^{-1}, depending on the rheological model. High shear rates, where blood is supposed to behave as a Newtonian fluid, can be found at the channel walls and can be even higher in the constriction region due to the presence of the obstacle. Figure 8-d qualitatively shows the shear rates across the channel width for the three regions. As can be observed, the shear rate is maximum around the obstacle and significantly reduces after it. Away from the constriction region, where higher viscosity values are expected, Newtonian models will tend to over-predict the results, which is in agreement with previous computational works carried out on intracranial aneurysm. (Xiang, Tremmel, Kolega, Levy, Natarajan, and Meng, 2012) Furthermore, overpredictions of these results might lead to incorrect estimations when studying thrombus generation or growth. (Lee, Chiu, and Jen, 1997)

Changes in the position of the maximum velocity also depends on the shear rate distribution. As

mentioned before, for the non-obstacle case maxima are expected to be at the channel center, because shear rates are equal at both channel walls. However, for the obstacle case, as can be appreciated in Fig. 4-b and Fig. 8-d (yellow line), shear rates at the obstacle and on the channel walls are different in magnitude producing a shift of the maximum position towards the surface of higher shear rates.

Due to the fact that blood clots, stents or thrombus might have different shapes. We consequently wanted to find out about the effect of the obstacle geometry on the flow. Thus, in addition to the semi-circular obstacle case, a rectangular shape with a height side equal to the semi-circle radius and a base equal to the semi-circle diameter was also considered. Figure 9 shows a comparison between the two geometries for the velocity profiles and an obstacle size of 40% of the channel width. Although a similar qualitative trend was found between the geometries, the velocity profiles for the semi-circular obstacle were $\sim 15\%$ higher.

Higher velocities are expected to be found for the semi-circular case since over this geometry the flow has an easier circulation and a lower reduction in the flow velocity. This behavior is found at all lengths and it is clearer at the channel outlet profile (blue line). The obtained differences show that the geometry has an effect, not only on the velocity magnitudes, but also on the location of the maximum velocity. Maximum velocities are closer to the top wall for the rectangular obstacle.

4. CONCLUSIONS AND PROSPECTS

In this work a quantitative comparison has been performed of blood flow using several rheological models in a normal blood channel as well as in the presence of an obstacle. A new methodology has
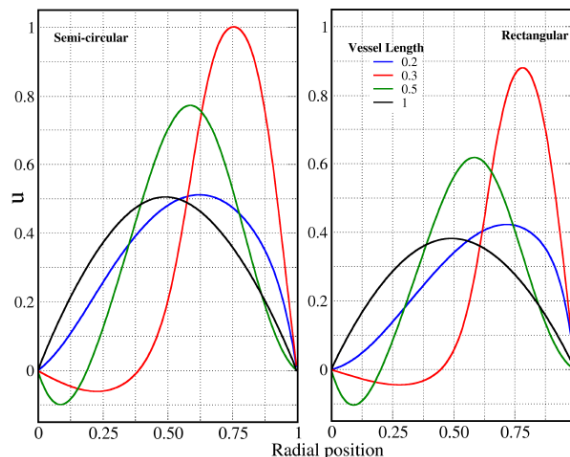
Fig. 9. Comparison of the Newtonian velocity profiles using a circular and rectangular geometry.

been proposed in order to simultaneously fit the parameters belonging to all the studied rheological models. Following this approach, a new set of parameters for the C-Y and the K-L models were determined based on several experimental samples for a wide range of shear rates. Additionally, it was found that the Casson model was unable to provide a good fit when a wide range of shear rates was included. This indicates that the C-Y and the K-L models should be considered as better alternatives. In our opinion any study needs to take into account a simultaneous fit of the parameters, otherwise, any comparison will be inconsistent.

Several physical observables have been studied, namely: velocity profiles, shear rate profiles and the length of the recirculation region. Among the studied rheological models, and regardless of the obstacle, the Newtonian model tends to predict higher numerical values for all the physical magnitudes. Although the C-Y and the K-L models show similar numerical results, the C-Y predictions were always larger than the K-L ones.

The presence of an obstacle produces for the studied Reynolds number: a reduction of the fluid velocities in the whole channel, a loss of symmetry with respect to the channel center, displacement of the velocity maxima and the appearance of a re-circulation region just after the obstacle. The location of the maximum velocity was found to be different between non-Newtonian and Newtonian models. The recirculation region length was found to be non-monotonically related to the obstacle size and the Newtonian models predicted the longest lengths. As a consequence, using Newtonian models might lead to predictions of higher probabilities of platelet adhesion to the wall channels and therefore higher probabilities of a thrombus growth.

The highest shear rate values were found over the obstacle region and were on average higher for the Newtonian model. Furthermore, once the obstacle was placed inside the channel there was a significant effect on the shear rate distribution. In fact, its behavior was found to be considerably different inside and outside the constriction region. For that

reason, a model with a constant viscosity might not be sufficient to provide a good system description and hence more detailed models should be used.

Despite the fact that the obstacle effect was included, it is known that a thrombus implies a complex set of chemical reactions that account for its formation and consequent growth. For that reason, a future study that considers these variables is needed. Additionally, the variables studied in this work are not enough to determine the best rheological model choice. Thus, in order to clarify this issue, more experimental information such as velocities or shear rates need to be also included.

5. ACKNOWLEDGMENTS

G. A. Orozco and D. A. Roa Romero, acknowledges the Universidad Antonio Nari~no for the financial support via the project number 2018-001.

REFERENCES

Anand, M. N., K. Rajagopal and K. R. Rajagopal (2005). A model for the formation and lysis of blood clots. *Pathophysiology of Haemostasis and Thrombosis* 34(2-3), 109–120.

Ashrafizaadeh, M. and H. Bakhshaei (2009). A comparison of non-newtonian models for lattice boltzmann blood flow simulations. *Computers and Mathematics with Applications* 58(5), 1045–1054.

Baskurt, O. K. and H. Meisleman (2003). Blood rheology and hemodynamics. *Seminars in Thrombosis and Hemostasis* 29(5), 436–450.

Bate, H. (1977). Blood viscosity at different shear rates in capillary tubes. *Biorheology* 14(5-6), 267–275.

Biro, G. P. (1982). Comparison of acute cardiovascular effects and oxygen-supply following haemodilution with dextran, stroma-free haemoglobin solution and fluorocarbon suspension. *Cardiovascular Research* 16(4),

194–204.

Bodnár, T., A. Sequeira and M. Prosi (2011). On the shear-thinning and viscoelastic effects of blood flow under various flow rates. *Applied Mathematics and Computation* 217(11), 5055–5067.

Box, F. M., R. J. van der Geest, M. C. M. Rutten and J. H. Reiber (2005). The influence of flow, vessel diameter, and non-newtonian blood viscosity on the wall shear stress in a carotid bifurcation model for unsteady flow. *Investigative Radiology* 40(5), 277–294.

Boyd, J., J. M. Buick and S. Green (2007). Analysis of the casson and carreauyasuda non-newtonian blood models in steady and oscillatory flows using the lattice boltzmann method. *Physics of Fluids* 19(9), 0931031–09310314.

Brooks, D., J. W. Goodwin and G. V. Seaman (1970). Interactions among erythrocytes under shear. *Journal of Applied Physiology* 28(2), 172–177.

Casson, N. (1959). A flow equation for pigment-oil suspensions of the printing ink type. In C. Mill (Ed.), *Rheology of Disperse Systems*, pp. 84–104. London, UK: Pergamon Press.

Chien, S. (1970). Shear dependence of effective cell volume as a determinant of blood viscosity. *Science* 168(3934), 977–979.

Chien, S., S. Usami, H. M. Taylor, J. L. Lundberg and and M. L. Gregersen (1966). Effects of hematocrit and plasma proteins on human blood rheology at low shear rates. *Journal of Applied Physiology* 21(1), 81–87.

Cho, I. Y. and R. K. Kensey (1991). Effects of the non-newtonian viscosity of blood on flows in a diseased arterial vessel. Part i: Steady flows. *Biorheology* 28(3-4), 241–262.

Fedosov, D. A., P. Wenxiao, B. Caswell, G. Gompper and G. E. Karnidiakis (2011). Predicting human blood viscosity in silico. *Proceedings of the National Academy of Sciences of the Unites States of America* 108(29), 11772–11777.

Fogelson, A. L. and R. D. Guy (2004). Platelet-wall interactions in continuum models of platelet thrombosis: formulation and numerical solution. *Mathematical Medicine and Biology* 21(4), 293–334.

Gijsen, F. J. H., E. Allanic, F. N. van de Vosse and J. Jansenn (1999). The influence of the non-newtonian properties of blood on the flow in large arteries: unsteady flow in a 90 curved tube. *Journal of Biomechanics* 32(7), 705–713.

Gijsen, F. J. H., F. N. van de Vosse and J. Jansenn (1999). The influence of the non-newtonian properties of blood on the flow in large arteries: steady flow in a carotid bifurcation model. *Journal of Biomechanics* 32(6), 601–608.

Glaser, R. (2012). *Biophysics, An Introduction.*

Heidelberg, Germany: Springer.

Ha, H. (2012). Hybrid piv-ptv technique for measuring blood flow in rat mesenteric vessels. *Microvascular Research* 84(3), 242–248.

Hathcock, J. (2006). Flow effects on coagulation and thrombosis. *Arteriosclerosis, Thrombosis, and Vascular Biology* 26(8), 1729–1737.

Krüger, T., F. Varnik and D. Raabe (2009). Shear stress in lattice boltzmann simulations. *Physical Review E* 79, 46704–1 – 46704–14.

Lee, D., Y. L. Chiu and C. Jen (1997). Platelet adhesion onto the wall of a flow chamber with an obstacle. *Biorheology* 34(12), 111–126.

Leuprecht, A. and K. Perktold (2001). Computer simulation of non-newtonian effects on blood flow in large arteries. *Computer Methods in Biomechanics and Biomedical Engineering* 4(2), 149–163.

Liu, Y. and W. K. Liu (2006). Rheology of red blood cell aggregation by computer simulation. *Journal of Computational Physics* 220(1), 139–154.

Lobanov, A. I. and T. K. Staroszhilova (2005). The effect of convective flows on blood coagulation processes. *Pathophysiology of Haemostasis and Thrombosis* 34(2-3), 121–134.

Luo, X. Y. and Z. B. Kuang (1992). A study of the constitutive equation of blood. *Journal of Biomechanics* 25(8), 929–934.

Milnor, W. R. (1982). *Hemodynamics*. Baltimore, MD: Willians and Wilkins.

Ouared, R. and B. Chopard (2005). Lattice boltzmann simulations of blood flow: non-newtonian rheology and clotting processes. *Journal of Statistical Physics* 121(1-2), 209–221.

Perktold, K., R. Peter and M. Resch (1995). Computer-simulation of local blood-flow and vessel mechanics in a compliant carotidartery bifurcation model. *Journal of Biomechanics* 28(7), 845–856.

Pivkin, I. V. and E. G. Karniadakis (2008). Accurate coarse-grained modeling of red blood cells. *Physical Review Letters* 101(11), 1181051–1181054.

Robertson, A. M., A. Sequeira and R. G. Owens (2009). Rheological models for blood. In L. Formaggia, A. Quarteroni, and A. Veneziani (Eds.), *Cardiovascular Mathematics*, Volume 1, Chapter 6, pp. 211–241. Milan, Italy: Springer-Verlag.

Skalak, R., S. R. Keller and T. W. Secomb (1981). Mechanics of blood flow. *Journal of Biomechanical Engineering* 103(2), 102–115.

Sorensen, E. N., G. W. Burgreen, W. R. Wagner and J. F. Antaki (1999a). Computational simulation of platelet deposition and activation: I. model development and properties. *Annals of*

Biomedical Engineering 27(4), 436–448.

Sorensen, E. N., G. W. Burgreen, W. R. Wagner and J. F. Antaki (1999b). Computational simulation of platelet deposition and activation: Ii. results for poiseuille flow over collagen. *Annals of Biomedical Engineering* 27(4), 449–458.

Succi, S. (2001). *The lattice Boltzmann method for fluid mechanics and beyond*. Oxford, UK: Clarendon Press.

Tangelder, G. J., D. W. Slaaf, A. M. Muijtjens, E. M. G. Arts, T., and R. S. Reneman (1986). Velocity profiles of blood platelets and red blood cells flowing in arterioles of the rabbit messentery. *Circulation Research* 59(5), 505–514.

Wang, C. H. and J. R. Ho (2011). A lattice Boltzmann approach for the non-newtonian effect in the blood flow. *Computers and Mathematics with Application* 62(1), 75–86.

Weller, F. F. (2008). Platelet deposition in non-parallel flow. *Journal of Mathematical Biology* 57(3), 333–359.

Weller, F. F. (2010). A free boundary problem modeling thrombus growth:modeling development and numerical simulations using the level set method. *Journal of Mathematical Biology* 61(6), 805–818.

Wootton, D. M., A. S. Popel and B. R. Alevriadou (2002). An experimental and theoretical study on the dissolution of mural fibrin clots by tissue-type plasmonigen activator. *Biotechnology and Bioengineering* 77(4), 405–419.

Xiang, J., M. Tremmel, J. Kolega, E. I. Levy, S. K. Natarajan and H. Meng (2012). Newtonian viscosity model could overesitmate wall shear stress in intracanial aneurysm domes and understimate rupture risk. *Hemorrhagic Stroke* 4(5), 351–357.

Xu, Z., N. Chen, M. M. Kamocka, E. D. Rosen, and M. Alber (2008). A multiscale model of thrombus development. *Journal of the Royal Society Interface* 5(24), 705–722.

Zhang, Z. W. and B. Neu (2009). Role of macro-molecular depletion in red blood cell adhesion. *Biophysics Journal* 97(4), 1031–1037.

Zou, Q. and X. He (1997). On pressure and velocity boundary conditions for the lattice boltzmann bgk model. *Physics of Fluids* 9, 1591–1598.

Zydney, A. L., J. D. Oliver III and C. K. Colton (1991). A constitutive equation for the viscosity of stored red cell suspensions: Effect of hematocrit, shear rate, and suspending phase. *Journal of Rheology* 35, 1639–1680.